AIAA-2001-4272

ISS LEAK LOCALIZATION USING ATTITUDE RESPONSE

Jong-Woo Kim,*
Department of Aerospace Engineering
Texas A&M University
College Station, TX 77843-3141

John L. Crassidis†
Department of Mechanical and Aerospace Engineering
University at Buffalo, The State University of New York
Amherst, NY 14260-4400

Srinivas R. Vadali‡
Department of Aerospace Engineering
Texas A&M University
College Station, TX 77843-3141

Adam L. Dershowitz§
United Space Alliance
NASA Johnson Space Center, Code DF64
Houston, TX 77058

ABSTRACT

This paper presents a new method to localize air leaks on the International Space Station based on the spacecraft attitude and rate behavior produced by a mass expulsion force of the leaking air. Thrust arising from the leak generates a disturbance torque, which is estimated using a real-time predictive filter with a dynamical model (including external disturbances such as aerodynamic drag and gravity-gradient). The leak location can be found by estimating the moment arm of the estimated disturbance torque, assuming that leak is caused by only one hole. Knowledge of the leak thrust magnitude and its resulting disturbance torque are needed to estimate the moment arm. The leak thrust direction is assumed to be perpendicular to the structure surface and its magnitude is determined using a Kalman filter with a nozzle dynamics model. There may be multiple leak locations for a given response, but the actual geometric structure of the space station eliminates many of the possible solutions. Numerical results show that the leak localization method is very efficient when used with the conventional sequential hatch closure or airflow induction sensor system.

INTRODUCTION

The International Space Station (ISS) is orbiting in a 51.6° inclination near-circular Low-Earth-Orbit (LEO) with an altitude between 370 and 460 km, and is expected to have a minimum operational lifetime of 15 years. Because of the large structure, long lifetime and orbit characteristics, the ISS may be subject to impacts of hyper velocity particles such as micrometeorites and space debris that can severely damage the station. This damage may threaten the safety of the crew if the pressurized wall of a module is perforated, which may result in significant air loss. Collisions with other objects are another possible cause of a leak, as occurred in the Russian Space Station Mir in 1997. To protect the ISS from the impact damages, various debris shields have been designed. Heavy shields are placed in the forward facing area which is likely to be hit frequently, and fewer shields are used in the nadir-facing and aft area.[1]

Perforations in a pressurized module will result in a rapid temperature and pressure decrease. Therefore

*Graduate Student, Student Member AIAA.
†Assistant Professor, Senior Member AIAA.
‡Professor, Associate Fellow AIAA.
§Flight Controller, Member AIAA.

fast determination of the extent and location of the leak is needed to maintain the operational status in order to provide safety for the crew. The first indication of a leak in the ISS is the depressurization of a module. The leak size can be calculated by measuring the internal pressure and its depressurization rate. Based on the extent of leak it is possible to calculate the "reserve time" left until a crew evacuation is required. Depending on the reserve time operational decisions must be made, including: 1) whether or not to perform a leak isolation to patch the leak, or 2) evacuate the ISS. Leak localization should be performed first to find the leaking module. Then the exact location within the leaking module for repair purposes can be determined.

Conventional methods to locate air leaks on the ISS include the sequential module leak isolation process for the US segment (prior to assembly stage 10A) and the airflow induction sensor system for the Russian segment. The sequential module leak isolation process involves having the crew close hatches sequentially while monitoring the pressure difference across each hatch. A drawback of this process is very small pressure differences can keep a closed hatch from being open again, which significantly reduces the reserve time and can pose an immediate risk to the crew. Thus, safety dictates that the hatches be closed in an order that will never trap a crew member away from the escape vehicle. This may significantly inhibit the leak isolation process if the leaking module is not located within the first few hatch closures.

The airflow induction sensor system employs hot-wire anenometers situated in hatchways to measure the air flow direction and its rate. The hot-wire anenometer operates by air passing across a wire with a current running through it to maintain a constant temperature in the wire. These devices are installed at all hatchways of the Russian segments. However, the airflow induction sensor system designed for the ISS has several limitations for the following reasons. The sensors are not mounted at all hatchways of the US segment (only at Node-2 and Node-3 of the US segment). Therefore the sequential module isolation process is still needed to determine which module leaks in the US segments. Since the sensors are very sensitive to the air circulation inside, the venting system and the movement of the crew must be stopped for several minutes, which may waste time in an emergency situation. Because these sensors are situated in hatchways, the location of the leak within the suspected leaking module cannot be found for repair purposes without using other inspection processes (this is also true for the sequential isolation process). Therefore a more efficient localization system is needed to locate the leaks.

The new method presented in this paper uses the attitude response of the ISS caused by the leak reaction force of the air flowing through a perforated hole. The leak force can yield a strong reaction torque depending on the size and location of the leak. A leak hole on the surface of a pressurized module can be modelled as a short nozzle with the leaking air as the propellant. We assume that the line of action of the leak force is perpendicular to the cross section area of the leak hole. This assumption is reasonable due to the relatively thin skin of each module. Based on the nozzle dynamics, an extended Kalman filter algorithm is used to estimate the leak force magnitude with the internal pressure measurements. The leak torque is estimated by a predictive filter[2] using attitude and rate measurements. Advantages of the predictive filter include: model errors are estimated as part of the filter solution, and online implementation of the estimation algorithm is possible. In this research, the leak torque is treated as a model error and is estimated by filtering the attitude and rate measurements. The possible locations of the air leak are then calculated using the estimated leak torque, leak force magnitude, and the actual geometric structure of the pressurized segments. For simplicity, the disturbance torque caused by the pressure of the impingement of the leaking air plume on nearby surfaces is neglected. Also, we assume that the leak is caused by a single leak hole.

There may be single or multiple leak locations that produce the same attitude response. To reduce the number of possible solutions, conventional methods are combined with the new leak localization method. This approach reduces the number of possible solutions, so that fewer hatch closures are required to uniquely determine the leak location. Advantages of the attitude response method include:

1. No other devices are needed besides pressure gauges to measure the air pressure, and spacecraft attitude and rate sensors.

2. Relatively fast leak localization can be achieved compared to the conventional leak localization method proposed for the ISS.

3. The new method not only determines the possible leaking modules but also determines the possible locations of the leak hole within those modules. This may be critical to allow for repairs rather than sealing off a module or performing a station evacuation.

The remainder of paper is organized as follows. First, the characteristics of the leaking air are shown using isentropic and isothermal nozzle models. Then the Kalman filter is derived for the calculation of the leak force magnitude. Next a summary of the attitude kinematics and dynamics for the ISS is given. Then a derivation is shown for the leak torque estimate using the predictive filter. Finally numerical simulations are

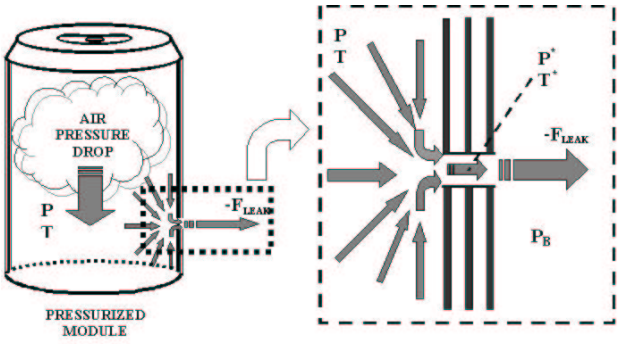

Fig. 1 Air Flow Through Leak Hole

presented and an example of the shuttle airlock depressurization effect on the ISS is shown using actual data.

LEAK FORCE

A leak hole perforated on the surface of a pressurized module will behave like a short length nozzle. The dynamic properties of the air flow through the leak hole are analyzed using one dimensional isentropic and isothermal nozzle dynamic models. Fig. 1 shows the diagram of the air flow through the leak hole on the pressurized module, where T^* and P^* are the temperature and pressure of the air in the leak hole, respectively, T and P are the temperature and pressure of the inside of the pressurized module, respectively, $\mathbf{F}_{LEAK}$ is the leak force, and P_B is the back pressure. The mass flow rate in a leak hole is given by[3]

$$\dot{m} = -\frac{AP^*v^*}{RT^*} \tag{1}$$

where A is the area of the hole, R is the ideal gas constant (287 N-m/Kg-K), and v^* is the exhaust velocity of the air satisfying

$$v^* = \sqrt{\gamma RT^*} \tag{2}$$

where γ is the specific heat ratio, with $\gamma = 1.4$ for an ideal gas. The mass flow rate $\dot{m}$ can be expressed as a function of the air inside the pressurized module. This is accomplished by substituting the following expressions into Eqn. (1):

$$P^* = P\left(\frac{2}{\gamma+1}\right)^{\frac{\gamma}{\gamma-1}} \tag{3a}$$

$$T^* = T\left(\frac{2}{\gamma+1}\right) \tag{3b}$$

yielding

$$\dot{m} = -\frac{AP\sqrt{\gamma}}{\sqrt{RT}}\left(\frac{2}{1+\gamma}\right)^{\frac{1+\gamma}{2(\gamma-1)}} \tag{4}$$

The actual mass flow rate can be calculated by multiplying $\dot{m}$ in Eqn. (1) by the discharge coefficient C_D. Using the thrust equation the leak force magnitude is given by

$$|\mathbf{F}_{LEAK}| = C_D\dot{m}v^* + (P^* - P_a)A \tag{5}$$

where P_a is the ambient pressure which is approximately zero for the vacuum of space. Substituting Eqns. (1), (2) and (3) into Eqn. (5), and simplifying yields

$$|\mathbf{F}_{LEAK}| = AP\left(C_D\gamma + 1\right)\left(\frac{2}{\gamma+1}\right)^{\frac{\gamma}{\gamma-1}} \tag{6}$$

Note that the magnitude of the leak force is proportional to the pressure inside the module and to the area of the leak hole. This expression is very useful since the leak force magnitude is a direct function of the internal pressure P, which can be measured by a pressure sensor. For the calculation of the hole area A the following approach is used. The indication of an air leak in a pressurized module is the depressurization of the air. The air inside the module follows the ideal gas law, given by

$$P = \frac{mRT}{V} \tag{7}$$

where V is the volume of the air. Differentiating Eqn. (7) with respect to time and using $\dot{m}$ from Eqn. (4) gives a depress rate model. Two kinds of depressurization process models are used, depending on the temperature characteristics of the air. For an isentropic air model, where P and T is related by

$$T = T_0\left(\frac{P}{P_0}\right)^{\frac{\gamma-1}{\gamma}} \tag{8}$$

the depressurization rate $\dot{P}$ is

$$\dot{P} = -k_1AP^{k_2} \tag{9a}$$

$$k_1 = \frac{\gamma\sqrt{RT_0\gamma}}{V}P_0^{\frac{1-\gamma}{2\gamma}}\left(\frac{2}{\gamma+1}\right)^{\frac{\gamma+1}{2(\gamma-1)}}C_D \tag{9b}$$

$$k_2 = \frac{3\gamma-1}{2\gamma} \tag{9c}$$

For an isothermal process, T is treated as a constant in Eqn. (7). Therefore the depressurization rate $\dot{P}$ can be derived as

$$\dot{P} = -k_3AP_0 \tag{10a}$$

$$k_3 = \frac{\sqrt{RT_0\gamma}}{V}\left(\frac{2}{1+\gamma}\right)^{\frac{1+\gamma}{2(\gamma-1)}}AP_0C_D \tag{10b}$$

where the subscript 0 stands for the initial value and, k_1, k_2 and k_3 are constants. Now, we can calculate the hole area A by measuring the internal pressure P and its depress rate $\dot{P}$.

Comparisons between the isentropic and isothermal gas model are shown in Figs. 2 and 3, using the ISS

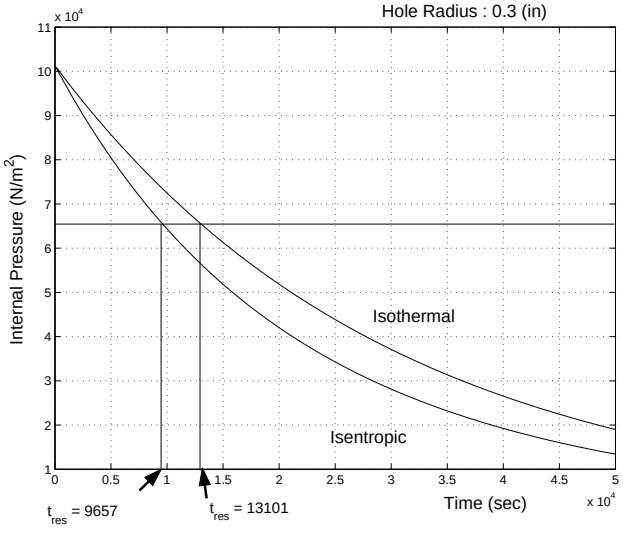

Fig. 2 Internal Pressure

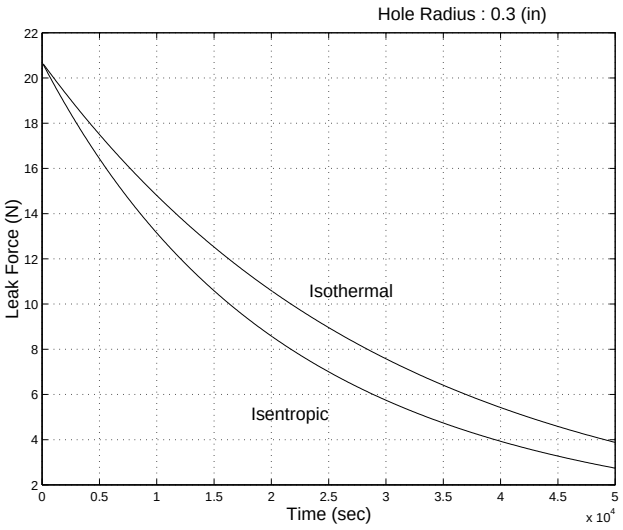

Fig. 3 Leak Force Magnitude

assembly Stage 16A with a leak hole radius of 0.3 inch. From Fig. 2, the isentropic gas model gives a faster pressure drop in the internal pressure than the isothermal gas model. Therefore the reserve time t_{res}, which is a measure of the time it takes for the current pressure P to reach the minimum habitable pressure $P_{min} \approx 490$ mmHg, is shorter using the isentropic gas model than using the isothermal gas model. The reserve time t_{res} can be obtained by integrating Eqn. (9b) for the isentropic process and Eqn. (10a) for the isothermal process. The reserve time for the isentropic process is

$$t_{res} = \frac{\left(\frac{P_{min}}{P}\right)^{\frac{1-\gamma}{2\gamma}} - 1}{\frac{\gamma-1}{2}\frac{A}{V}\sqrt{RT\gamma}\left(\frac{2}{\gamma+1}\right)^{\frac{\gamma+1}{2(\gamma-1)}} C_D} \tag{11}$$

where the internal temperature T can be substituted by P from Eqn. (8). From Fig. 3 the leak force magnitude is larger using the isothermal gas model, meaning the isothermal gas model produces a greater torque than the isentropic gas model. If the leak area hole size is small then the isothermal model can be used (since the temperature will remain fairly constant), otherwise the isentropic model should be used.

Estimation of Leak Force Magnitude

Since the actual internal pressure measurements are corrupted by noise, the Kalman filter[4] is used to estimate the hole area which is needed to calculate the magnitude of leak force. The state equations for the depressurization process have the following form

$$\dot{\mathbf{x}}(t) = \mathbf{f}\left[\mathbf{x}(t), t\right] + \boldsymbol{\eta}(t) \tag{12}$$

where the state $\mathbf{x}(t) = [P(t),\ A(t)]^T$ and

$$\mathbf{f}\left[\mathbf{x}(t), t\right] = \begin{bmatrix} -k_1 A P^{k_2} \\ 0 \end{bmatrix} \tag{13}$$

for an isentropic process model, and

$$\mathbf{f}\left[\mathbf{x}(t), t\right] = \begin{bmatrix} -k_3 A P \\ 0 \end{bmatrix} \tag{14}$$

for isothermal process model. The vector $\boldsymbol{\eta} = [\eta_1,\ \eta_2]^T$ is the process noise vector, where η_1 and η_2 are Gaussian white-noise processes with

$$E\left\{\eta_i(t)\right\} = 0 \tag{15a}$$

$$E\left\{\eta_i(t)\eta_j(t')\right\} = Q_i \delta_{i,j}(t - t') \tag{15b}$$

with $i,\ j = 1,\ 2$. The matrix Q_i has the following form

$$Q = \begin{bmatrix} \sigma_1^2 & 0 \\ 0 & \sigma_2^2 \end{bmatrix} \tag{16}$$

where the terms σ_1^2 and σ_2^2 are the variances of η_1 and η_2, respectively. The internal pressure measurement is modelled as

$$\tilde{z}_k = h_k\left[\mathbf{x}(t_k)\right] + v_k, \quad k = 1,\ 2,\ \ldots,\ m \tag{17a}$$

$$h_k\left[\mathbf{x}(t_k)\right] = P_k, \quad k = 1,\ 2,\ \ldots,\ m \tag{17b}$$

where m is the number of measurements and v_k is the measurement noise which satisfies a discrete Gaussian white-noise process with

$$E\left\{v_k\right\} = 0 \tag{18a}$$

$$E\left\{v_k v_{k'}\right\} = R_k \delta_{k,k'} \tag{18b}$$

The propagation of the state satisfies

$$\dot{\hat{\mathbf{x}}}(t) = \mathbf{f}\left[\hat{\mathbf{x}}(t), t\right] \tag{19a}$$

$$\hat{z}_k = h_k\left[\hat{\mathbf{x}}(t_k)\right] \tag{19b}$$

where $\hat{\mathbf{x}}(t) = [\hat{P}(t),\ \hat{A}(t)]^T$ is the state estimate vector. The error covariance propagation matrix $\mathcal{P}$ satisfies

$$\dot{\mathcal{P}}(t) = F\left[\hat{\mathbf{x}}(t), t\right]\mathcal{P}(t) + \mathcal{P}(t)F\left[\hat{\mathbf{x}}(t), t\right]^T + Q \tag{20}$$

where $F[\hat{\mathbf{x}}(t), t]$ is given by

$$F[\hat{\mathbf{x}}(t), t] = \left.\frac{\partial \mathbf{f}[\mathbf{x}(t), t]}{\partial \mathbf{x}(t)}\right|_{\mathbf{x}=\hat{\mathbf{x}}} \tag{21a}$$

$$= \begin{bmatrix} -k_1 k_2 \hat{A} \hat{P}^{k_2-1} & -k_1 \hat{P}^{k_2} \\ 0 & 0 \end{bmatrix} \tag{21b}$$

for an isentropic process, and

$$F[\hat{\mathbf{x}}(t), t] = \left.\frac{\partial \mathbf{f}[\mathbf{x}(t), t]}{\partial \mathbf{x}(t)}\right|_{\mathbf{x}=\hat{\mathbf{x}}} \tag{22a}$$

$$= \begin{bmatrix} -k_3 \hat{A} & -k_1 \hat{P} \\ 0 & 0 \end{bmatrix} \tag{22b}$$

for an isothermal process.

The state estimate and error covariance updates are given by

$$\hat{\mathbf{x}}_k^+ = \hat{\mathbf{x}}_k^- + K_k \left[\tilde{z}_k - h_k(\hat{\mathbf{x}}_k^-)\right] \tag{23a}$$

$$\mathcal{P}_k^+ = \left[I - K_k H_k(\hat{\mathbf{x}}_k^-)\right] \mathcal{P}_k^- \tag{23b}$$

where the superscript $(+)$ stands for the updated value and $(-)$ stands for the a priori value. The Kalman gain matrix is given by

$$K_k = \mathcal{P}_k^- H_k(\hat{\mathbf{x}}_k^-)^T \left[H_k(\hat{\mathbf{x}}_k^-) \mathcal{P}_k^- H_k(\hat{\mathbf{x}}_k^-)^T + R_k\right]^{-1} \tag{24}$$

where $H_k(\hat{\mathbf{x}}^-)$ is the measurement sensitivity matrix, given by

$$H_k(\hat{\mathbf{x}}_k^-) = \left.\frac{\partial h_k(\mathbf{x}(t_k)^-)}{\partial \mathbf{x}(t_k)}\right|_{\mathbf{x}=\hat{\mathbf{x}}} = \begin{bmatrix} 1 & 0 \end{bmatrix} \tag{25}$$

Thus with the use of the internal pressure measurements the extended Kalman filter algorithm can be used to estimate the leak hole area. Then the magnitude of leak force can be calculated by substituting the estimated values of $\hat{P}$ and $\hat{A}$ into Eqn. (6).

ISS ATTITUDE DYNAMICS MODEL

In this section the attitude kinematics and dynamics of the ISS in the presence of external disturbances in LEO are derived. For the attitude kinematics, the quaternion is used to specify the attitude of the ISS.[5] The quaternion is defined as

$$\mathbf{q} \equiv \begin{bmatrix} \mathbf{q}_{13} \\ q_4 \end{bmatrix} \tag{26}$$

where the vector part $\mathbf{q}_{13}$ is

$$\mathbf{q}_{13} \equiv \begin{bmatrix} q_1 \\ q_2 \\ q_3 \end{bmatrix} = \hat{\mathbf{n}} \sin\left(\frac{\theta}{2}\right) \tag{27}$$

and the scalar part q_4 is

$$q_4 = \cos\left(\frac{\theta}{2}\right) \tag{28}$$

where $\hat{\mathbf{n}}$ is a unit vector indicating the principal rotation axis and θ is the principal rotation angle. The quaternion components satisfy the following normalization constraint

$$\mathbf{q}^T \mathbf{q} = q_1^2 + q_2^2 + q_3^2 + q_4^2 = 1 \tag{29}$$

The quaternion kinematic equations of motion are given by

$$\dot{\mathbf{q}} = \frac{1}{2} \Omega(\boldsymbol{\omega}) \mathbf{q} \tag{30}$$

where $\boldsymbol{\omega}$ is the angular velocity and Ω is defined as

$$\Omega(\boldsymbol{\omega}) \equiv \begin{bmatrix} -[\boldsymbol{\omega}\times] & \vdots & \boldsymbol{\omega} \\ \cdots\cdots\cdots\cdots & & \\ -\boldsymbol{\omega}^T & \vdots & 0 \end{bmatrix} \tag{31}$$

where $[\boldsymbol{\omega}\times]$ represents the skew-symmetric matrix, defined by

$$[\boldsymbol{\omega}\times] \equiv \begin{bmatrix} 0 & -\omega_3 & \omega_2 \\ \omega_3 & 0 & -\omega_1 \\ -\omega_2 & \omega_1 & 0 \end{bmatrix} \tag{32a}$$

If the attitude quaternion $\mathbf{q}$ represents the orientation of the body reference frame with respect to the Local-Vertical-Local-Horizontal (LVLH) orbital reference frame then the velocity vector $\boldsymbol{\omega} = \boldsymbol{\omega}_{B/L}$ is given by

$$\boldsymbol{\omega}_{B/L} = \boldsymbol{\omega}_{B/N} + n\mathbf{C}_2(\mathbf{q}) \tag{33}$$

where $\boldsymbol{\omega}_{B/N}$ is the angular velocity with respect to an inertial frame, $\mathbf{C}_i$ is the i^{th} column of the coordinate transformation matrix from the LVLH orbital reference frame to the body reference frame, and n is the orbital frequency of the spacecraft.[6]

The dynamic equations of rotational motion of a rigid spacecraft in a LEO environment are given by Euler's equation:

$$\dot{\mathbf{H}} = -\left[J^{-1}(\mathbf{H} - \mathbf{h})\right]\times\mathbf{H} + \mathbf{N}_{DRAG} + \mathbf{N}_{GRAV} + \mathbf{d}_{LEAK} \tag{34}$$

where $\mathbf{H}$ is the total angular momentum of the spacecraft satisfying

$$\mathbf{H} = J\boldsymbol{\omega} + \mathbf{h} \tag{35}$$

and J is the inertia matrix, $\mathbf{N}_{DRAG}$ is the aerodynamic torque, $\mathbf{N}_{GRAV}$ is the gravity gradient torque, $\mathbf{h}$ is the angular momentum of the control moment gyroscopes (CMGs), and $\mathbf{d}_{LEAK}$ is the leak torque. Other environmental effects such as solar radiation and Earth's albedo are neglected. Also the effects caused by internal moving parts such as solar array rotations are omitted for simplicity at this point (solar array models will be included in future studies since the resultant torques produced by the arrays may be significant).

The gravity-gradient torque for a circular orbiting spacecraft is given by

$$\mathbf{N}_{GRAV} = 3n^2 \mathbf{C}_3(\mathbf{q}) \times J\,\mathbf{C}_3(\mathbf{q}) \tag{36}$$

The aerodynamic torque $\mathbf{N}_{DRAG}$ is modelled such that the drag force and the center of pressure location are functions of the attitude of the spacecraft:

$$\mathbf{N}_{DRAG} = -\frac{1}{2}\rho_a v_a^2 C_D S \left[\boldsymbol{\rho}_{cp} \times \mathbf{C}_1(\mathbf{q})\right] \tag{37}$$

where v_a is the magnitude of the atmospheric velocity with respect to the spacecraft, which can be approximated as the circular orbital speed. The atmospheric density ρ_a is assumed constant, which is not completely true because of the diurnal heating effect of the Earth's atmosphere. The drag coefficient C_D is assumed to be constant for a given orientation of the spacecraft. Also, S is the attitude dependent frontal area and $\boldsymbol{\rho}_{cp}$ is the attitude dependent center of pressure location. A method to determine the attitude dependent aerodynamic parameters has been developed in Ref. [6], where the reference area and the center of pressure are calculated for any orientation by defining interpolation functions. The projected area and the center of pressure for the three orthogonal body reference axes of the ISS are given in Ref. [7] for each assembly stage.

The leak torque is modelled by

$$\mathbf{d}_{LEAK} = \mathbf{R}_{LEAK} \times \mathbf{F}_{LEAK} \tag{38}$$

where $\mathbf{R}_{LEAK}$ is the moment arm of a leak torque from the center of mass of the spacecraft to a leak location, and $\mathbf{F}_{LEAK}$ is a leak force. The leak torque is unknown and will be estimated by treating it as a model error in the predictive filter, explained in the next section.

LEAK TORQUE ESTIMATION

In this section a nonlinear predictive filter is derived to estimate the leak torque. It is assumed that measurements of attitude ($\tilde{\mathbf{q}}$), angular rate ($\tilde{\boldsymbol{\omega}}$) and CMG momentum ($\mathbf{h}$) are available. The leak torque is treated as a to-be-determined model error using the available measurements in the predictive filter (see Ref. [8] for a detail derivation of the predictive filter). The state equations for the filter are

$$\dot{\hat{\mathbf{q}}} = \frac{1}{2}\Omega\left[J^{-1}\left(\hat{\mathbf{H}} - \mathbf{h}\right) + n\mathbf{C}_2(\hat{\mathbf{q}})\right]\hat{\mathbf{q}} \equiv \mathbf{f}_{\hat{\mathbf{q}}}\left(\hat{\mathbf{q}}, \hat{\mathbf{H}}\right) \tag{39a}$$

$$\begin{aligned}\dot{\hat{\mathbf{H}}} = &-\left[J^{-1}\left(\hat{\mathbf{H}} - \mathbf{h}\right)\right] \times \hat{\mathbf{H}} \\ &+ \mathbf{N}_{DRAG} + \mathbf{N}_{GRAV} + \mathbf{d}_{LEAK} \\ &\equiv \mathbf{f}_{\hat{\mathbf{H}}}\left(\hat{\mathbf{q}}, \hat{\mathbf{H}}\right)\end{aligned} \tag{39b}$$

where the hat denotes the estimated value. The output estimate equation is given by

$$\hat{\mathbf{y}}\left(\hat{\mathbf{q}}, \hat{\mathbf{H}}\right) \equiv \left[\hat{\mathbf{y}}_1^T, \hat{\mathbf{y}}_2^T\right]^T = \begin{bmatrix} \hat{\mathbf{q}} \\ \cdots\cdots\cdots\cdots \\ J^{-1}\left(\hat{\mathbf{H}} - \mathbf{h}\right) \end{bmatrix} \tag{40}$$

where the lowest order of the time derivative in which $\hat{\mathbf{d}}_{LEAK}$ first appears is 2 for $\hat{\mathbf{y}}_1$ and 1 for $\hat{\mathbf{y}}_2$. Note that

$$\hat{\mathbf{y}}_2 = J^{-1}\left(\hat{\mathbf{H}} - \mathbf{h}\right) = \hat{\boldsymbol{\omega}} \tag{41}$$

Using the notation of Ref. [9] and performing the filter derivation with Eqns. (39a), (39b) and (40), gives the following equation for the leak torque estimate:

$$\begin{aligned}\hat{\mathbf{d}}_{LEAK} = &-\left\{S[\hat{\mathbf{x}}(t)]^T \Lambda(\Delta t) R^{-1} \Lambda(\Delta t) S[\hat{\mathbf{x}}(t)] + W\right\} \\ &\times S[\hat{\mathbf{x}}(t)]^T \Lambda(\Delta t) R^{-1}\left\{\mathbf{z}[\hat{\mathbf{x}}(t)] - \tilde{\mathbf{y}}(t + \Delta t) + \hat{\mathbf{y}}(t)\right\}\end{aligned} \tag{42}$$

where $\hat{\mathbf{x}}(t) \equiv [\hat{\mathbf{q}}^T, \hat{\mathbf{H}}^T]^T$, Δt is the sampling interval, $\tilde{\mathbf{y}} \equiv [\tilde{\mathbf{q}}^T, \tilde{\boldsymbol{\omega}}^T]^T$, and

$$\Lambda = \frac{1}{2}\begin{bmatrix} \Delta t^2 I_{4\times4} & \vdots & 0_{4\times3} \\ \cdots\cdots\cdots\cdots & \cdots & \cdots\cdots \\ 0_{3\times4} & \vdots & 2\Delta t I_{3\times3} \end{bmatrix} \tag{43}$$

The matrix $S(\hat{\mathbf{x}})$ can be derived as

$$S(\hat{\mathbf{x}}) = \begin{bmatrix} \frac{1}{2}\Xi(\hat{\mathbf{q}})J^{-1} \\ \cdots\cdots\cdots \\ J^{-1} \end{bmatrix} \tag{44}$$

where $\Xi(\hat{\mathbf{q}})$ is defined as

$$\Xi(\hat{\mathbf{q}}) \equiv \begin{bmatrix} q_4 I_{3\times3} + [\hat{\mathbf{q}}_{13}\times] \\ \cdots\cdots\cdots\cdots\cdots \\ -\mathbf{q}_{13}^T \end{bmatrix} \tag{45a}$$

$$\hat{\mathbf{q}}_{13} = \begin{bmatrix} q_1, & q_2, & q_3 \end{bmatrix}^T \tag{45b}$$

Also, the matrix R is given by

$$R = \begin{bmatrix} \sigma_q^2 I_{4\times4} & \vdots & 0_{4\times3} \\ \cdots\cdots\cdots\cdots & \cdots & \cdots\cdots \\ 0_{3\times4} & \vdots & \sigma_\omega^2 I_{3\times3} \end{bmatrix} \tag{46}$$

where the scalars σ_q^2 and σ_ω^2 are the variances of the measurement error processes of $\tilde{\mathbf{q}}$ and $\tilde{\boldsymbol{\omega}}$, respectively. The vector $\mathbf{z}$ in Eqn. (42) is given by

$$\mathbf{z} = \begin{bmatrix} \mathbf{z}_{\hat{\mathbf{q}}} \\ \cdots \\ \mathbf{z}_{\hat{\mathbf{H}}} \end{bmatrix} \tag{47}$$

$$\mathbf{z}_{\hat{\mathbf{q}}} = \Delta t\, \mathbf{f}_{\hat{\mathbf{q}}} + \frac{1}{2}\Delta t^2\left(\frac{\partial \mathbf{f}_{\hat{\mathbf{q}}}}{\partial \hat{\mathbf{q}}}\,\mathbf{f}_{\hat{\mathbf{q}}} + \frac{\partial \mathbf{f}_{\hat{\mathbf{q}}}}{\partial \hat{\mathbf{H}}}\,\mathbf{f}_{\hat{\mathbf{H}}}\right) \tag{48a}$$

$$\mathbf{z}_{\hat{\mathbf{H}}} = \Delta t\, \mathbf{f}_{\hat{\mathbf{H}}} \tag{48b}$$

Therefore, given a state estimate at time t, Eqn. (42) is used to process the measurement $\tilde{\mathbf{y}}$ at time $t+\Delta t$ to find $\hat{\mathbf{d}}_{LEAK}(t)$ to be used in $[t, t+\Delta t]$ to propagate the state estimate to time t using Eqns. (39a), (39b) and (40). The weighting matrix W serves to weight the relative importance between the propagated model and measured quantities. If this matrix is set to zero, then no weight is placed on minimizing the model corrections so that a memoryless estimator is given.

LEAK LOCALIZATION

Once a leak torque $\mathbf{d}_{LEAK}$ is estimated by the predictive filter, the next step involves determining the position vector $\mathbf{R}_{LEAK}$, which is the moment arm of the leak torque satisfying

$$\mathbf{d}_{LEAK} = \mathbf{R}_{LEAK} \times \mathbf{F}_{LEAK} \tag{49}$$

In the above equation, the leak torque $\mathbf{d}_{LEAK}$ and the magnitude of $\mathbf{F}_{LEAK}$ are known by the estimation algorithms. The overall steps for locating a leak on the ISS are as follows:

1. Model the 3 dimensional geometric surfaces of the pressurized parts of the spacecraft.

2. Estimate the leak torque and magnitude of the leak force.

3. Slice the 3-D surfaces of the pressurized modules with a plane perpendicular to the direction of the leak torque so that this plane comprises the center of mass of the spacecraft. From the fundamental definition of torque, a torque about the center of mass of a rigid body is perpendicular to the plane comprising the vectors $\mathbf{R}_{LEAK}$ and $\mathbf{F}_{LEAK}$. So, $\mathbf{R}_{LEAK}$, $\mathbf{F}_{LEAK}$ and the center of mass are all in the same plane normal to the direction of the leak torque. Denote this plane by τ. The intersection between the plane τ and the surface of the spacecraft produces contours.

4. With the assumption that the leak force is normal to the tangent plane of the partial section on the ISS surface where the leak occurs, calculate the gradient vectors (direction normal vectors) of the points that make up the sliced contours obtained in Step 3.

5. Multiply the magnitude of the leak force estimated in Step 1 with all gradient vectors calculated in Step 4.

6. Since the position and gradient vectors of all the points making the sliced contours are known, calculate the resulting torque at each point on the contours.

7. From the torques obtained for each point in Step 6, select the torques that are closest to the estimated torque (within an error bound) and check their points on the contours.

The actual geometric structure of the station eliminates many of the possible solutions; however, multiple solutions may still exist. In this case further assumptions can be made, such as the probability of impacts by the debris or small meteorites is low on the aft and nadir facing surfaces since these surfaces are shaded by other structures. Also, the leak localization method based on the attitude response may be combined with the conventional leak localization methods. For example, if the solution shows two leaks situated at two different modules then only one hatch closure between any of these modules is needed to check which one of the two modules leaks. Furthermore, visual inspections by the crew may narrow the possible leak solutions.

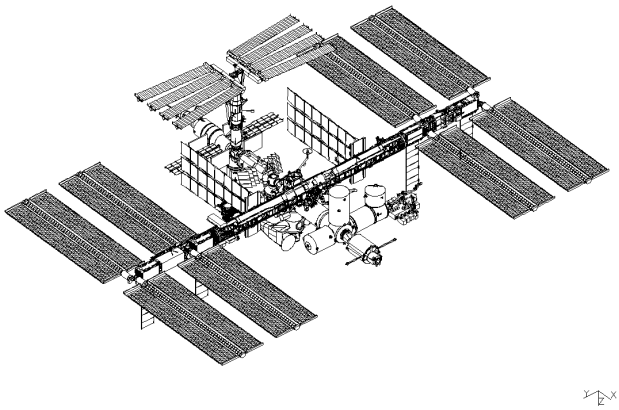

Fig. 4 ISS Assembly Stage 16A, Ref. [7]

NUMERICAL SIMULATION

A numerical algorithm coded in MATLAB has been developed to test the performance of the leak localization method for various situations. For the simulation, the ISS assembly Stage 16A with the nominal Earth-pointing operation mode is considered. Fig. 4 shows the configuration of the ISS. A MATLAB 3-D surface model of the pressurized segment of the ISS Stage 16A has been developed based on the data provided in Ref. [7]. The isentropic depressurization process of the air inside the ISS is assumed, with a true leak hole radius of 0.3 inch. The mass and aerodynamic properties of the ISS are also provided in Ref. [7]. The true mass M and inertia J are given by

$$M = 469682\,(\text{kg}) \tag{50}$$

$$J = \begin{bmatrix} 127908568 & 3141229 & 7709108 \\ 3141229 & 107362480 & 1345279 \\ 7709108 & 1345279 & 200432320 \end{bmatrix} (\text{kg m})^2 \tag{51}$$

The centers of pressure are given by $\boldsymbol{\rho}_{cpx} = [0, -0.355, -0.927]^T$ m, $\boldsymbol{\rho}_{cpy} = [-7.94,\ 0, -1.1]^T$ m and $\boldsymbol{\rho}_{cpz} = [1.12,\ 0.247,\ 0]^T$ m in the Space Station Analysis Coordinate System (SSACS) with respect to the center of mass. The components x, y and z represent the three orthogonal axes of the ISS body fixed frame.[7] The reference projected areas are $S_x = 967$ m^2, $S_y = 799$ m^2 and $S_z = 3525$ m^2.

The Global Positioning System (GPS) attitude-sensor measurement-error standard deviation is given by $\sigma_q = 0.17$ deg, and the ring-laser gyro sensor measurement-error standard deviation is given by

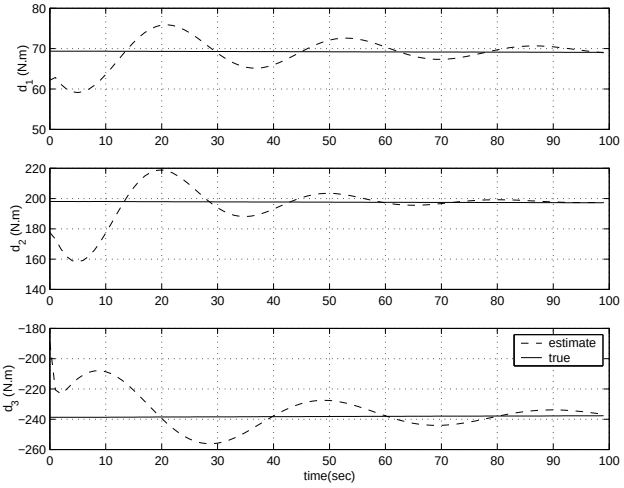

Fig. 5 True and Estimated Leak Torque

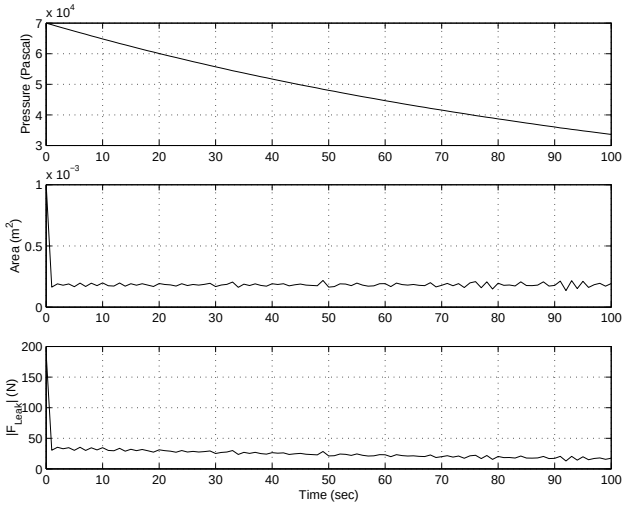

Fig. 6 Leak Force Magnitude and Hole Area Estimate

$\sigma_\omega = 4\times10^{-4}$ deg/sec.[10] The measurement-error standard deviation of the internal pressure is given by $\sigma = 0.1$ mmHg. For the depressurization of the air inside, the initial internal temperature and pressure are set to $T_0 = 21^o$ C and $P_0 = 1$ atm, respectively. The back pressure is assumed to be $P_B = 0$ atm, and the volume of the entire pressurized system is $V = 867.2$ m^3. Finally, an inertia uncertainty of 3% is added to the true inertia J.

Simulations are done for 100 seconds from the start of the leak. The true and estimated leak torques (determined by the predictive filter) are shown Fig. 5. Transients are present in the predictive filter, which are due to model inaccuracies; however, as will be seen, the leak localization algorithm is fairly robust even with such large transient errors. Fig. 6 shows the estimate of the leak hole area using the Kalman filter algorithm. The true leak hole area A is $1.8241 * 10^{-4}$ m^2. As seen from this figure the Kalman filter accurately estimates the leak hole area. The leak force magnitude is then computed with the internal pressure measurement and the estimate of the hole area.

For the first simulation a leak is assumed on a module shown in Fig. 7. The sliced plane τ with contours in 3-D is shown in Fig. 8. Using the leak localization approach a single leak has been determined for this simulated case, depicted in Fig. 9. The estimated position is marked with a $\circ$, the true position of a leak is marked with a $*$ for comparison, and the center of mass is marked with a $\star$ on the plane τ. Slicing of the 3-D surface is performed at the end of the simulation ($t = 100$ sec). If no errors are present in the assumed model and if the assumptions made so far are perfectly satisfied, then the closest torque yielding the point to the estimated leak torque is the true leak point. But because of sensor inaccuracies and modelling errors in the inertia, the estimated leak torque may deviate from the true value. Therefore, an upper error bound should be set when selecting points that

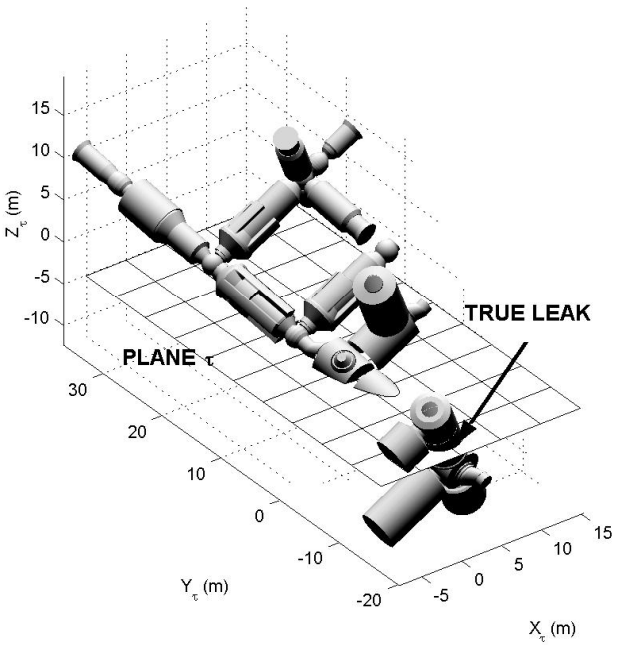

Fig. 7 Slicing 3-D Surface Model with Plane τ

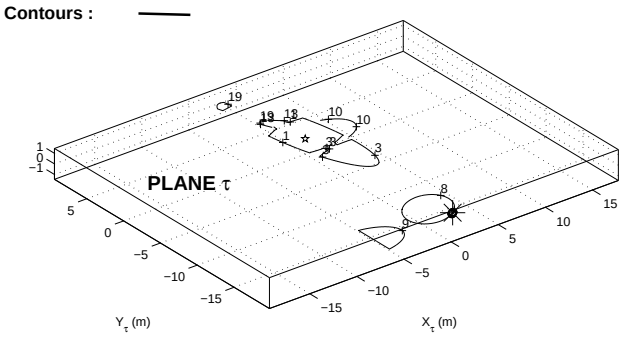

Fig. 8 Sliced Plane τ with Contours in 3-D

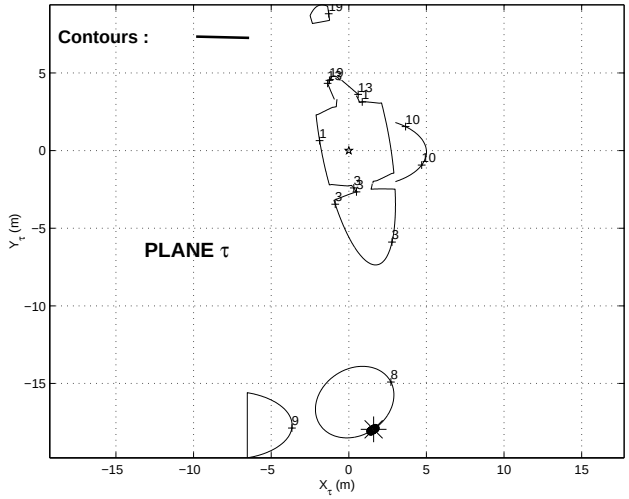

Fig. 9 Contours on Plane τ with Possible Leak

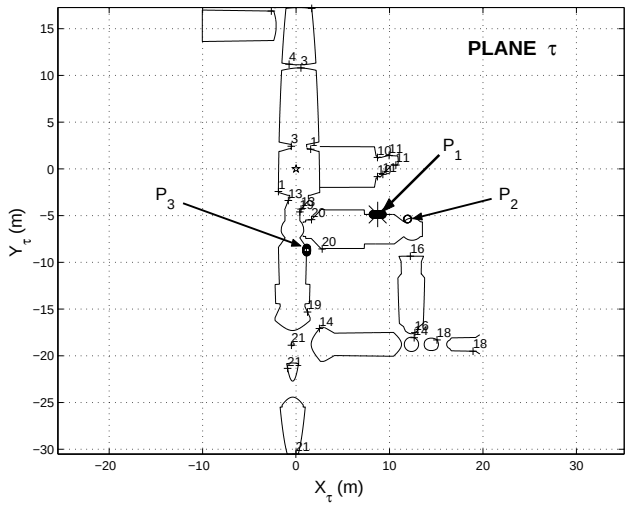

Fig. 10 Contours on Plane τ with 3 Possible Leaks

yield the torque closest to the estimated leak torque. For the case shown in Figure 9, we conclude that the leak occurs on the contour line labelled 8, which corresponds to the Kibo JEM pressurized module. In this simulated case, the leak location is well estimated using the new localization method.

Another simulation has been done where multiple locations may result from the given estimated leak torque. In this case the estimated leak locations are spread over several modules, as shown in Fig. 10. The locations P_1, P_2 and P_3 are possible leak candidates (the true leak point is situated near P_1). But since P_1 and P_2 are on the same module, a crew person only needs to close one hatch between the module labelled 20 and the module labelled 19 to verify which one of the two modules has a leak. This is accomplished by measuring the internal pressure drop rate or using visual inspections of the estimated leak points. If the leak hole is due to space debris or small meteorite punctures, then the aft and nadir facing surfaces of the ISS have little possibility to be impacted. This is also true for locations where regions are protected by other structures, as is the case for point P_3. Therefore this point is not a likely candidate for the leak.

Initial results indicate that the leak localization method may be sensitive to modelling errors, such as the spacecraft mass properties and aerodynamic parameters. These values may vary with time; especially for the aerodynamic parameters which are coupled with orbit position and solar activity. Therefore, a robust parameter estimation method should be employed to exactly estimate these parameters. Several methods have been proposed for on-line parameter identification of the ISS.[6] Also the effect of the disturbance torque caused by the pressure of the impingement of the leaking air plume on nearby surfaces may be a critical source of disturbance when a leak occurs. Because of inherent complexities, analyzing these effects may be difficult. A proposed method involves determining a residual model error, which includes all the aforementioned effects, using the predictive filter when it is known that a leak does not occur. Then, assuming that the residual error is small for the next orbit, this model error is subtracted from the new estimated model error in the next orbital pass. If no leak is determined, then a new residual error is determined and the process continues until a leak is found.

AIRLOCK DEPRESSURIZATION

The effects of the air vent on the attitude of the ISS assembly Stage 5A with the mated Space Shuttle (STS-98) is investigated in this section (see Fig. 11). The purpose of this section is to estimate the torque and the upper bound magnitude of the force caused by the air vent from the depressurization of the Space Shuttle airlock for the preparation of extravehicular activity (EVA) of the crew. The actual data are recorded from 2001, 045, 09h 30min (GMT) through 2001, 045, 15h 40min (GMT), and airlock depressurization started around 14h 30min. Because a T-shaped valve is used (see Fig. 12), where air is vented on opposite sides of the valve structure, the net thrust should be nullified in theory. But if the expelled air is not uniform at both openings a net thrust may occur. In the present case, from Fig. 13, the CMG momentum buildup occurs during the pressurization process which means that the net thrust is not cancelled.

In preparation for an EVA, two stages are needed to depressurize the Space Shuttle external airlock:

1. The airlock is depressurized from 703 hPa to 345 hPa. The valve is open until 345 hPa is reached and then closed to maintain 345 hPa.

2. The valve is reopened with the valve diameter increased to depressurize the airlock from 345 hPa to 0 hPa.

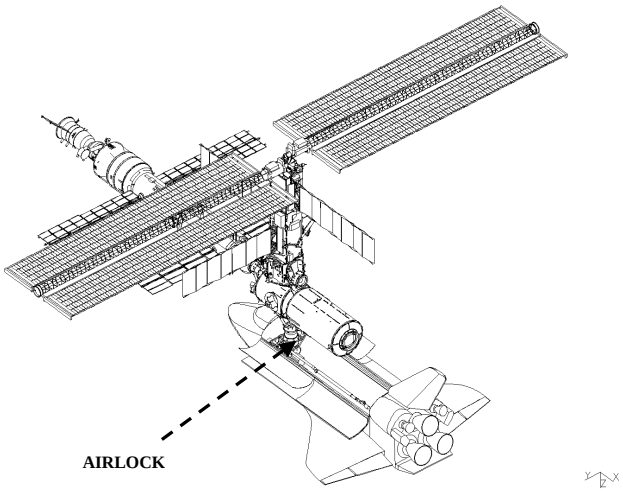

Fig. 11 ISS mated with Space Shuttle Atlantis, Stage 5A Intermediate 2, Ref. [7]

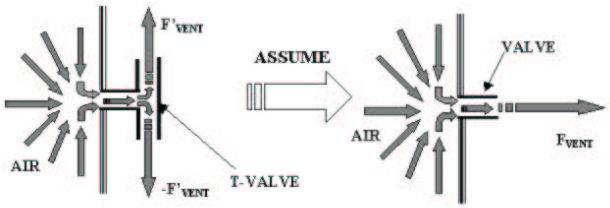

Fig. 12 External Airlock of Space Shuttle and Depress Valve

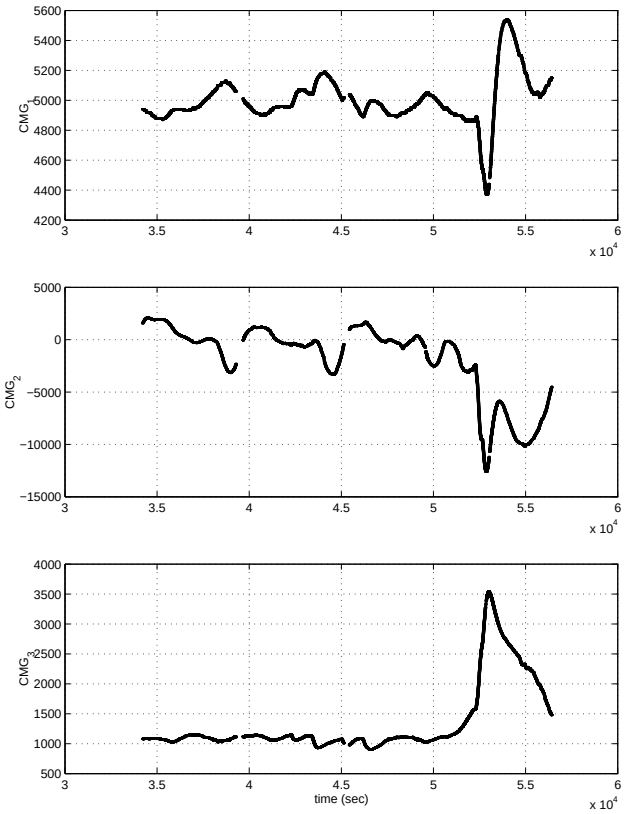

Fig. 13 CMG Angular Momentum

Figure 14 shows the pressure and temperature measurements in the airlock, where depressurization occurs at t = 52240 sec (note that t = 0 corresponds to t = 2001, 045, 00h 00min 00sec in GMT). Airlock depressurization starts at around 52240 seconds. The magnitude of the vent force caused by the venting air is estimated based on the following assumptions:

1. Depressurization of the airlock follows an isothermal process based on the internal temperature history.

2. A single straight opening valve is used (although a T-shaped valve is used in reality).

3. No air flow decelerations occur inside the valve (dA = 0), but the hole area A is not required to be a constant.

Only the upper bound magnitude of the vent force can be given because of the assumption made in 2. We can assume that the temperature inside the airlock is nearly constant around 18^o C based on Fig. 14. Fig. 15 shows the results obtained from the Kalman filter algorithm. The figures are re-scaled to show the depressurization part in detail. The pressure data closely follows the predicted depress process of the EVA explained earlier. The estimated hole area varies

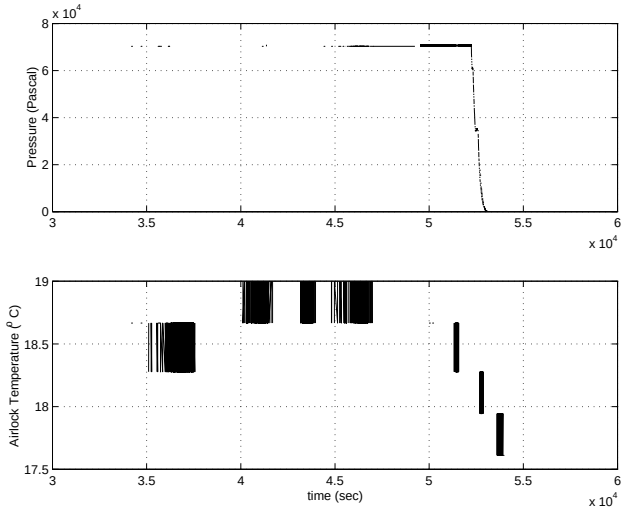

Fig. 14 Pressure and Temperature in Airlock

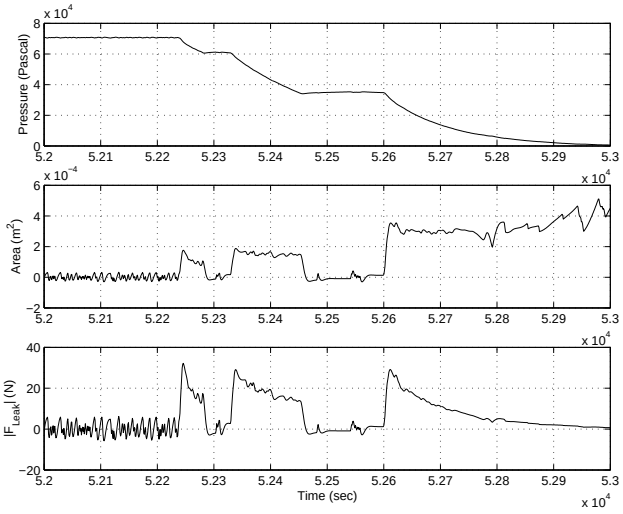

Fig. 15 Hole Area and Vent Force Magnitude Estimate

between 1×10^{-4} m^2 to 3×10^{-4} m^2, which corresponds to 0.56 cm (0.22 in) and 1 cm (0.4 in) in hole radius, respectively. Note that the computed valve area does not reveal the actual one because of the assumptions in 2. Therefore from the results shown in Fig. 15, only an upper bound of the exit area of the valve can be obtained. This is not ideal case for this research since the external airlock of the Space Shuttle is situated inside the Space Shuttle cargo bay with the depressurization valve at its bottom part, which probably interacted with surfaces near the airlock valve. Furthermore the geometry of the T-shaped valve makes the analysis more complicated. However, the obtained results are consistent with intuitive assumptions.

CONCLUSIONS

In this paper a new leak localization method using the attitude response is developed for the International Space Station. The leaking air through the perforated hole on the external surface area leads to a reaction force which results in a torque affecting the attitude of the spacecraft. The size of the leak was calculated using estimated values from a Kalman filter of the internal air pressure and area of the leak hole. The resultant leak torque was estimated by a nonlinear predictive filter algorithm. The actual geometric structure of the space station eliminates many of the possible solutions, but multiple solutions may still exist. This was overcome by combining the new method presented in this paper with conventional methods. Numerical results showed that the proposed leak localization method determines the location of the leak rapidly and precisely. Furthermore, actual test data from a depressurization of the Space Shuttle airlock indicates that the proposed method has the potential to accurately estimate the leak hole size and venting force magnitude.

ACKNOWLEDGEMENT

This work has been supported by a grant from United Space Alliance (contract number C00-00109). This support is greatly appreciated.

REFERENCES

[1] *Protecting the Space Station from Meteoroids and Orbital Debris*, National Research Council, Washington, D.C., 1997.

[2] Crassidis, J. L., "Robust Control of Nonlinear Systems Using Model-Error Control Synthesis," *Journal of Guidance, Control, and Dynamics*, Vol. 22, No. 4, 1999, Jul.-Aug., pp. 595–601.

[3] Sonntag, R. E., Borgnakke, C., and Wylen, G. J. V., *Fundamentals of Thermodynamics*, John Wiley & Sons, Inc., New York, 5th ed., 1998.

[4] Gelb, A., editor, *Applied Optimal Estimation*, MIT Press, Cambridge, Mass., 1974.

[5] Crassidis, J. L., Markley, F. L., Anthony, T. C., and Andrews, S. F., "Nonlinear Predictive Control of Spacecraft," *Journal of Guidance, Control, and Dynamics*, Vol. 20, No. 6, Nov.-Dec. 1997, pp. 1096–1103.

[6] Carter, M. T. and Vadali, S. R., "Parameter Identification for the International Space Station Using Nonlinear Momentum Management Control," *AIAA-97-3524*, August 1997.

[7] *International Space Station On-Orbit Assembly, Modeling, and Mass Properties Databook: Design Analysis Cycle Assembly Sequence, JSC-26557, Rev. J*, Lockheed Martin, Cambridge, Mass., 5th ed., 1999.

[8] Crassidis, J. L. and Markley, F. L., "Predictive Filtering for Nonlinear Systems," *Journal of Guidance, Control, and Dynamics*, Vol. 20, No. 3, May-June 1997, pp. 566–572.

[9] Crassidis, J. L. and Markley, F. L., "Predictive Filtering for Attitude Estimation Without Rate Sensors," *Journal of Guidance, Control, and Dynamics*, Vol. 20, No. 3, May-June 1997, pp. 522–527.

[10] *United States Control Module Guidance, Navigation, and Control Subsystem Design Concept*, NASA MSFC-3677, Al., March 1997.